Molecular Imaging of Fibrin Deposition in Deep Vein Thrombosis Using Fibrin-Targeted Near-Infrared Fluorescence

Tetsuya Hara, MD, PHD,* Brijesh Bhayana, PHD,† Brian Thompson, PHD,*†‡
Chase W. Kessinger, PHD,* Ashok Khatri, PHD,§ Jason R. McCarthy, PHD,‡
Ralph Weissleder, MD, PHD,‡ Charles P. Lin, PHD,†‡ Guillermo J. Tearney, MD, PHD,†
Farouc A. Jaffer, MD, PHD*†

Boston, Massachusetts

OBJECTIVES The goal of this study was to develop and validate a new fibrin-targeted imaging agent that enables high-resolution near-infrared fluorescence (NIRF) imaging of deep vein thrombosis (DVT).

BACKGROUND NIRF imaging of fibrin could enable highly sensitive and noninvasive molecular imaging of thrombosis syndromes in vivo.

METHODS A fibrin-targeted peptide was conjugated to a near-infrared fluorophore Cy7, termed FTP11-Cy7. The NIRF peptide is based on a fibrin-specific imaging agent that has completed Phase II clinical magnetic resonance imaging trials. In vitro binding of FTP11-Cy7 to human plasma clots was assessed by using fluorescence reflectance imaging. Next, FTP11-Cy7 was intravenously injected in mice with femoral DVT induced by topical 7.5% ferric chloride treatment. Intravital fluorescence microscopy and noninvasive fluorescence molecular tomography–computed tomography were performed in 32 mice with DVT, followed by histological analyses.

RESULTS In vitro human clot-binding analyses showed a 6-fold higher NIRF clot target-to-background ratio (TBR) of FTP11-Cy7 than free Cy7 (6.3 ± 0.34 vs. 1.2 ± 0.03; p < 0.0001). The thrombus TBR of acute and subacute femoral DVT with FTP11-Cy7 obtained by using intravital fluorescence microscopy was >400% higher than control free Cy7. Binding of FTP11-Cy7 to thrombi was blocked by a 100-fold excess of unlabeled competitor peptide both in vitro and in vivo (p < 0.001 for each). Histological analyses confirmed that FTP11-Cy7 specifically accumulated in thrombi. Noninvasive fluorescence molecular tomography–computed tomography imaging of fibrin in jugular DVT demonstrated strong NIRF signal in thrombi compared with sham-operated jugular veins (mean TBR 3.5 ± 0.7 vs. 1.5 ± 0.3; p < 0.05).

CONCLUSIONS The fibrin-targeted NIRF agent FTP11-Cy7 was shown to avidly and specifically bind human and murine thrombi, and enable sensitive, multimodal intravital and noninvasive NIRF molecular imaging detection of acute and subacute murine DVT in vivo. (J Am Coll Cardiol Img 2012; 5:607–15) © 2012 by the American College of Cardiology Foundation

Thrombosis and thromboembolic diseases such as myocardial infarction, stroke, pulmonary embolism, and deep vein thrombosis (DVT) are major causes of morbidity and mortality worldwide (1). Clinical detection of thrombosis syndromes often uses ultrasound, x-ray computed tomography (CT), or magnetic resonance imaging (MRI). However, such imaging approaches require the presence of a relatively large thrombus to render a diagnosis of a thrombotic disorder. In many cases (e.g., plaque rupture, stent thrombosis, early or resolving DVT), a much more

sensitive measure of early thrombosis is required. Furthermore, thrombus detection for most current imaging modalities is structurally related to the cessation of blood flow. It could therefore prove beneficial to harness a molecular marker of fibrin to characterize thrombus or microthrombus type/composition and to guide fibrinolytic therapy of fibrin-rich thrombi.

Fibrin, a trimeric molecule consisting of alpha-, beta-, and gamma-chains, is present in both arterial and venous thrombi at micromolar concentrations and is minimally present in the circulating blood, rendering it a favorable imaging target for in vivo detection (2). Previous studies have investigated fibrin-targeted agents for nuclear imaging (3,4) and more recently, a fibrin-specific gadolinium-based agent (EP-2104R) for MRI (5-8) that has been tested in clinical trials (9,10).

However, only a few robust fibrin-targeted agents exist for in vivo optical, and specifically, near-infrared fluorescence (NIRF), imaging. Attractive features of NIRF imaging include high-resolution imaging capabilities (11), as well as noninvasive (12) and intravascular (13,14) imaging platforms. In addition, fluorescence-based detection is inherently more sensitive than MRI-based detection and thus requires lower dosages and shorter washout times for injected agents (15).

In this study, we synthesized and investigated the avidity and specificity of a new fibrin-targeted NIRF thrombus imaging agent termed FTP11-Cy7. We report here the targeting capabilities and specificity of the NIRF agent in acute and subacute murine DVT by using high-resolution intra-vital fluorescence microscopy (IVFM) and noninvasive integrated fluorescence molecular tomography (FMT)–computed tomography (CT) in vivo.

METHODS

Synthesis of FTP11-Cy7, a NIRF fibrin-targeted imaging agent. The fibrin-targeted fluorescent peptide (FTP11-Cy7) was synthesized in the MGH Peptide/Protein Core facility using solid-phase chemistry-based on EP-2104R (8), a peptide imaging agent comprising 11 amino acids (Tyr-D-Glu-Cys-Hyp-Tyr [3-Cl]-Gly-Leu-Cys-Tyr-Ile-Gln-NH$_2$), and cyclized via the formation of a disulphide bond (8). Full synthesis details are provided in the Online Appendix. Linearity of the NIRF signal intensity generated from FTP11-Cy7 was assessed by using fluorescence reflectance imaging (FRI) at various concentrations (sample volume of 50 μl).

In vitro clot binding. Human plasma clots were created from fresh-frozen plasma (FFP) in 96 well plates (16). FFP was obtained using an institutional review board–approved human subject protocol. Each well received 90 μl of FFP, 5 μl of 0.4 M CaCl$_2$, and 5 μl of thrombin (0.1 U/μl phosphate-buffered saline [PBS]). The plate was incubated at 37°C for 90 min to clot the plasma. Thereafter, 0.02 nmol of fluorophore was added to respective wells and then incubated at 37°C for an additional 30 min. In competitive binding assays, unlabeled FTP11 at 10-fold or 100-fold excess concentration was added 30 min before the incubation of FTP11-Cy7 with clots. The clots were then washed twice with PBS and centrifuged at 500 rpm for 10 min. They were then washed twice more with PBS and imaged by using FRI (excitation/emission 740/790 nm). Experiments were performed in quadruplicate.

Animal studies. Animal studies were approved by the Hospital Subcommittee of Research Animal Care. For in vivo studies, C57BL/6 mice were anesthetized using an intraperitoneal ketamine (50 mg/ml [330 μl]), xylazine (100 mg/ml [50 μl]), and sterile saline (380 μl) mixture. Each mouse received a 50-μl intraperitoneal induction dose of the resulting mixture, followed by a 10- to 20-μl intraperitoneal dose hourly for continued anesthesia.

Blood half-life study of FTP11-Cy7. To determine the blood half-life of FTP11-Cy7, serial blood sampling was performed through a jugular vein. C57BL/6 mice (n = 5) received a 150 nmol/kg intravenous bolus of the FTP11-Cy7 dissolved in PBS. At the desired time points, a 50-μl volume of blood was obtained and mixed with 50 μl of heparin (1,000 USP units/ml) and kept on ice until

analysis. The Cy7 fluorescence of the blood at each time point was quantified by using FRI. The blood NIRF signal at each time point was measured and then normalized by the NIRF signal at 1 min post-injection. Exponential fitting yielded the blood half-life of FTP11-Cy7 (GraphPad Prism 5.0, San Diego, California).

Creation of DVT in mice. In vivo DVT were induced by topical ferric chloride injury to the femoral vein (for IVFM studies) or jugular vein (for FMT studies) (17). Under anesthesia, ferric chloride was locally applied to the vein using a 1-mm strip of Whatman No. 1 filter paper soaked in 7.5% ferric chloride. The filter paper was applied to the anterior surface of the vein for 5 min. Thereafter, the filter paper was removed, and the surgical field was irrigated with PBS. For acute imaging studies, imaging was performed in 2-h-old DVT. For subacute imaging studies, imaging was performed in 3-day-old (72-h) DVT. A total of 32 mice were studied.

Intravital fluorescence microscopy. To image fibrin deposition in thrombi at high-resolution, IVFM of femoral DVT was performed in 23 mice. Mice were anesthetized as noted earlier. At 60 min before imaging, a fibrin-targeted agent (FTP11-Cy7, n = 5 acute DVT; n = 5 subacute DVT) or control agent (free Cy7, n = 5) was administered via retro-orbital injection. Agents were injected at a dose of 150 nmol/kg in 100 μl of total volume. In in-vivo blocking experiments (n = 8), unlabeled FTP11 (1,500 nmol/kg) or PBS was injected 30 min before injection of FTP11-Cy7 (15 nmol/kg). Injection of 100 μl of fluorescein-labeled dextran (fluorescein isothiocyanate [FITC]-dextran, Sigma, St. Louis, Missouri; 5 mg/ml; excitation/emission 490/520 nm) provided an angiogram. IVFM studies used a multichannel laser scanning fluorescence microscope optimized for intravital imaging (18). The utilized 30× objective (NA 0.9) provided an in-plane resolution of 1.4 μm/pixel. Z stacks (20 to 40 slices) were obtained at 5-μm steps through the vessel. All image settings were kept constant for all time points and samples.

FMT-CT. Noninvasive integrated FMT-CT was performed as previously described (19) in 9 mice with subacute jugular vein DVT. FTP11-Cy7 was injected intravenously at 150 nmol/kg mouse 1 h before imaging. The surgical incisions remained closed during imaging. The NIRF signal was detected with a FMT 2500 system (excitation/emission 745 nm/785 nm, Perkin Elmer, Waltham, Massachusetts). To identify thrombosed and sham-

operated jugular veins, CT venograms were obtained via continuous infusion of iodinated contrast (Isovue-370, Bracco Diagnostics Inc., Princeton, New Jersey; rate 55 μl/min via tail vein). To enable accurate co-registration between FMT and CT datasets, an imaging cartridge containing the anesthetized mouse was placed into a custom-machined Plexiglas holder that supplied isoflurane, warm air, and optimal positioning in the CT scanner (Inveon PET-CT, Siemens, Knoxville, Tennessee). FMT-CT co-registration was performed by using OsiriX shareware. Fiducials on the imaging cartridge were visualized and tagged in FMT and CT images, allowing point-based co-registration in OsiriX (19).

Fluorescence reflectance imaging. Plasma clots, blood samples, and resected vessels underwent FRI with a near-infrared (NIR) filter set (excitation/emission 740/790 nm; Kodak ImageStation 4000, Carestream Health, Inc., Rochester, New York). Multiple exposure times (0.1 to 60 s) generated images that were exported to 16-bit unscaled TIFF files for further analysis with ImageJ version 1.44o (Bethesda, Maryland).

Image analyses. Image analyses of IVFM datasets were performed by summation of Z stacks into a 2-dimensional summation image with ImageJ. Thrombi presented as filling defects on FITC-dextran–generated angiograms. Regions-of-interest of the thrombus and the adjacent normal vessel were manually traced (11). Reconstruction and image analysis of FMT-CT datasets were performed with OsiriX version 3.5.1 software (64 bit) (19). Target-to-background ratios (TBRs) were calculated by dividing the mean region-of-interest signal of target by the mean region-of-interest signal of the background (PBS-treated clot, adjacent vessel, or other organs).

Histopathology. After sacrifice, mice were perfused with 0.9% saline (20 ml) via the left ventricle. For histopathologic analysis, femoral vessels were excised and embedded in optimal cutting temperature compound (Sakura Finetek, Torrance, California). Serial 6-μm cryostat sections were obtained for fluorescence microscopy. Adjacent sections were stained with hematoxylin and eosin for general morphology. NIR fluorescence microscopy was performed on fresh-frozen femoral vein sections using an upright epifluorescence microscope (Nikon Eclipse 90i; Tokyo, Japan). Fluorescence images were obtained in the NIR channel for FTP11-Cy7 (excitation/emission 710/810 nm; exposure time 50 ms), and FITC channel for autofluorescence (excitation/emission 480/535 nm; exposure time 50 ms).

Statistical analysis. Results are expressed as mean ± SEM. Statistical comparisons between 2 groups were evaluated by using the Mann-Whitney *U* test and the Kruskal-Wallis test for multiple groups followed by the Dunn post-test. Statistical comparisons and half-life calculations were performed with GraphPad Prism. A p value <0.05 was considered statistically significant.

RESULTS

Synthesis of FTP11-Cy7, a NIRF fibrin-imaging agent. A schematic representation of the FTP11-Cy7 is shown in Figure 1A. The high-performance liquid chromatography trace demonstrated $>98\%$ purity (Fig. 1B). The final product showed a molecular mass of 2062 g/mol using matrix-assisted laser desorption/ionization mass spectrometry (Fig. 1C), in agreement with the calculated mass. The NIRF signal of the FTP11-Cy7 peptide, as measured by using FRI, related linearly to its Cy7 concentration at concentrations relevant for imaging (Fig. 1D) ($R^2 = 0.99$).

In vitro binding assessment of FTP11-Cy7 to human plasma clots. The binding ability of FTP11-Cy7 was first evaluated in vitro in human FFP clots. After 30 min of incubation with individual agents, NIRF signals were measured by using FRI (Fig. 2). In vitro clot-binding analyses showed $>500\%$ higher clot TBRs for FTP11-Cy7 compared with control free Cy7 (6.3 ± 0.34 vs. 1.2 ± 0.03; $p < 0.0001$). An excess of unlabeled competitor peptide significantly blocked binding of FTP11-Cy7 in a dose-dependent manner (TBR 5.0 ± 0.45 for 10-fold excess, 2.5 ± 0.34 for 100-fold excess), indicating that the engineered NIRF peptide was clot specific.

Blood half-life of FTP11-Cy7. Blood clearance was assessed by serial blood sampling in mice (n = 5), followed by measurement of blood NIRF signal levels with FRI. The NIRF signal decreased rapidly from the blood, with a blood half-life of 2.82 min (95% confidence interval: 1.85 to 5.90) (Fig. 3).

High-resolution IVFM of fibrin in femoral DVT. To determine whether FTP11-Cy7 could enable high-resolution imaging of fibrin deposition, murine femoral DVT were imaged by using IVFM. Both acute DVT (2-h-old) and subacute DVT (3-day-old) were studied. Thrombi were identified as filling defects on FITC-dextran angiograms. IVFM demonstrated that NIRF signal increased in both acute and subacute thrombi (Figs. 4A and 4B). In contrast, control free Cy7 did not enhance thrombi
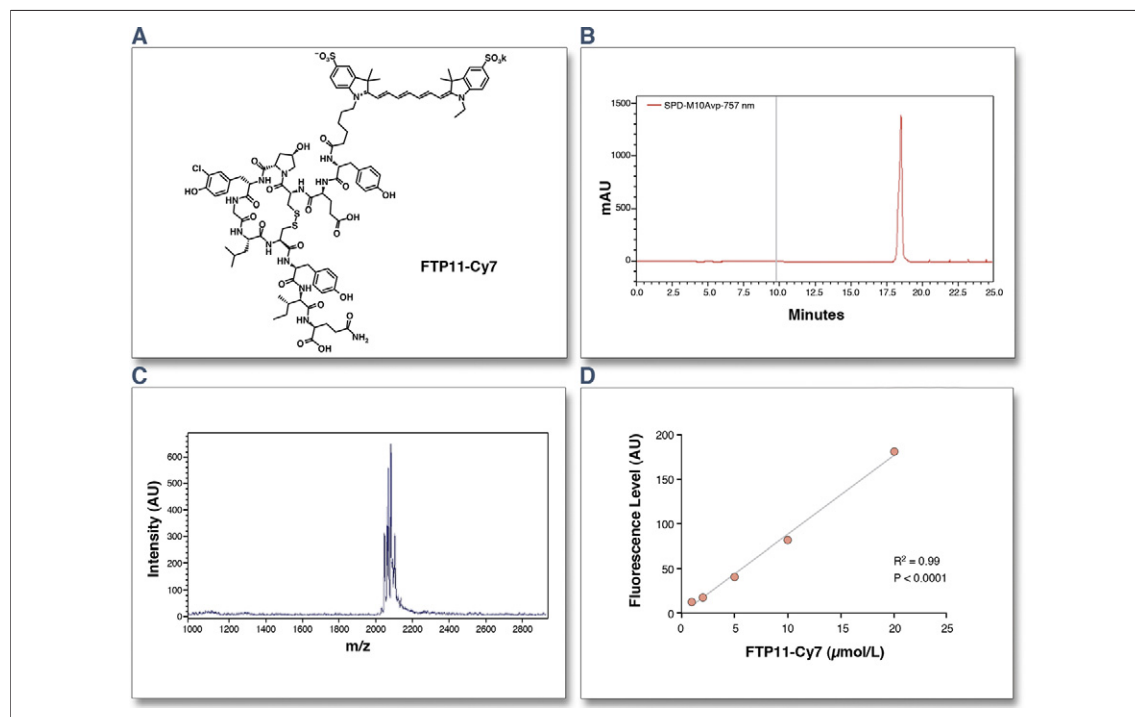

Figure 1. Synthesis and Structure of FTP11-Cy7

(A) FTP11-Cy7 is composed of 11 amino acids conjugated to the near-infrared fluorochrome, Cy7. **(B)** The high-performance liquid chromatography trace demonstrates $>98\%$ purity. **(C)** Matrix-assisted laser desorption/ionization mass spectrometry shows a molecular mass of 2062 g/mol. **(D)** The near-infrared fluorescence signal of the FTP11-Cy7 related linearly to its Cy7 concentration ($R^2 = 0.99$).

(Fig. 4C). The thrombus TBR was significantly higher in the FTP11-Cy7 groups (3.5 ± 0.3 for acute DVT, 2.7 ± 0.5 for subacute DVT; 0.46 ± 0.08 for free Cy7) (Fig. 4D). We also performed in vivo blocking experiments to evaluate the in vivo binding specificity of FTP11-Cy7. Pre-injection of 100-fold excess of unlabeled FTP11 blocked the FTP11-Cy7–mediated NIRF signal enhancement of acute DVT (thrombus TBR 1.6 ± 0.11 vs. 0.99 ± 0.04 blocked group; p < 0.001) (Fig. 4E). Fluorescence microscopy and hematoxylin and eosin staining of the histological sections demonstrated the accumulation of NIRF signal in DVT in the FTP11-Cy7 group (Figs. 5A and 5B). In contrast, control free Cy7 did not enhance thrombi (Fig. 5C).

Noninvasive FMT-CT of FTP11-Cy7 accumulation in jugular DVT. To image fibrin deposition in DVT noninvasively, we next performed FMT-CT of thrombosed jugular veins of mice. The same mice also possessed a sham-operated contralateral right jugular vein. To assess FMT signals accurately, we co-registered fiducially matched jugular veins from FMT and anatomic CT images (Figs. 6A to 6C). The TBR of the left jugular DVT was 230% higher than the sham-operated right jugular vein (mean TBR 3.5 ± 0.7 vs. 1.5 ± 0.3; p < 0.05) (Fig. 6D).

After FMT-CT, jugular veins were resected, and ex vivo FRI was performed. High NIRF signal was noted in the DVT of the mice (Figs. 7A and 7B). The TBR of the thrombosed vein was higher than that of the sham-operated right jugular vein (3.9 ± 0.4 vs. 2.4 ± 0.4; p < 0.05) (Fig. 7C).

DISCUSSION

In this investigation, we demonstrated the following: 1) the synthesis and specificity validation of a new human and murine fibrin-targeted imaging agent for in vivo NIRF imaging; 2) high-resolution, efficient IVFM detection of fibrin deposition, in both acute and subacute murine DVT; and 3) noninvasive detection of fibrin-rich jugular DVT using integrated FMT-CT.

The fibrin-targeted NIRF agent is based on the peptide backbone of EP-2104R (8), an MRI agent that has successfully undergone Phase II clinical trials (9,10) and therefore seems attractive for clinical translation. Another favorable capability of the fibrin-targeted NIRF agent is the ability to detect thrombi with >20-fold lower injected dose (150 nmol/kg) compared with other MRI-based thrombosis imaging agents (4 to 10 μmol/kg) (6,10,20).
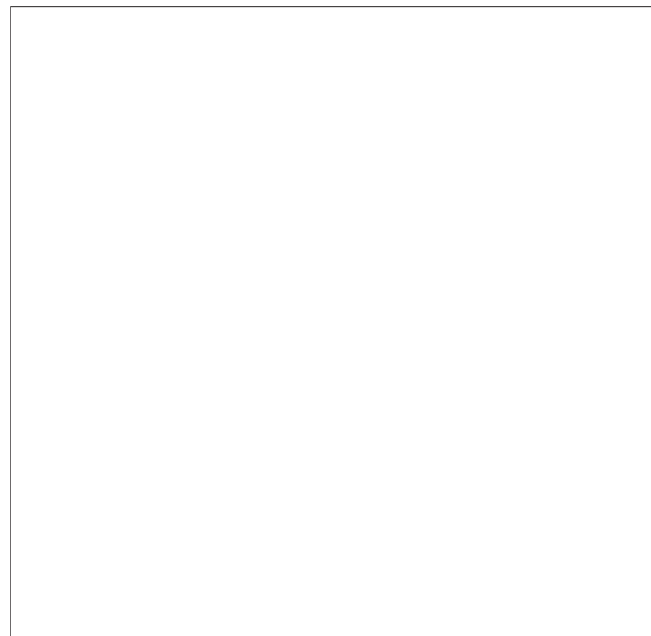
Figure 2. NIRF Imaging of Fibrin in Human Plasma Clots

(A) Clots incubated with FTP11-Cy7 showed a 6-fold increase (p < 0.0001) in near-infrared fluorescence (NIRF) signal enhancement compared with free Cy7. The NIRF signal was significantly blocked with an excess of competitor peptide in a dose-dependent manner. **(B)** Representative light and NIRF images of in vitro binding of FTP11-Cy7 to human plasma clots obtained by fluorescence reflectance imaging. *p < 0.05, ***p < 0.0001. **Bars** represent mean ± SE. PBS = phosphate-buffered saline; TBR = target-to-background ratio.
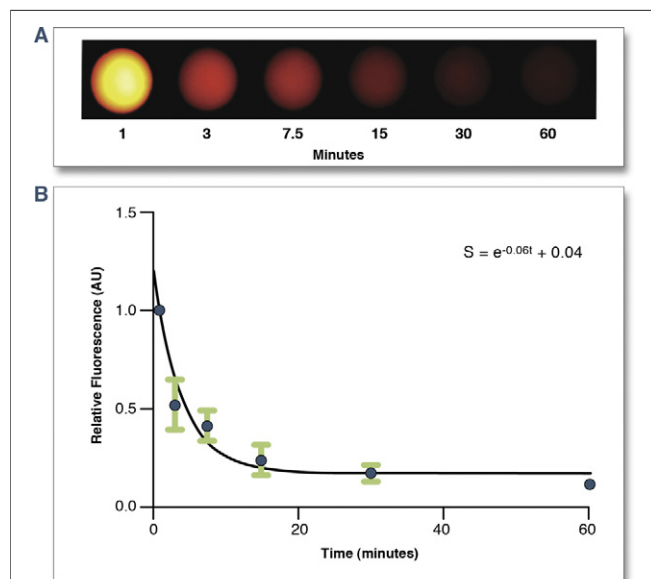

$$S = e^{-0.06t} + 0.04$$

Figure 3. Clearance of FTP11-Cy7 in Blood Circulation

After injecting FTP11-Cy7 via tail vein in normal C57BL/6 mice, serial blood sampling was performed through jugular vein. **(A)** Cy7 levels were measured by using fluorescence reflectance imaging. **(B)** The blood half-life was 2.8 min (95% confidence interval: 1.85 to 5.90).
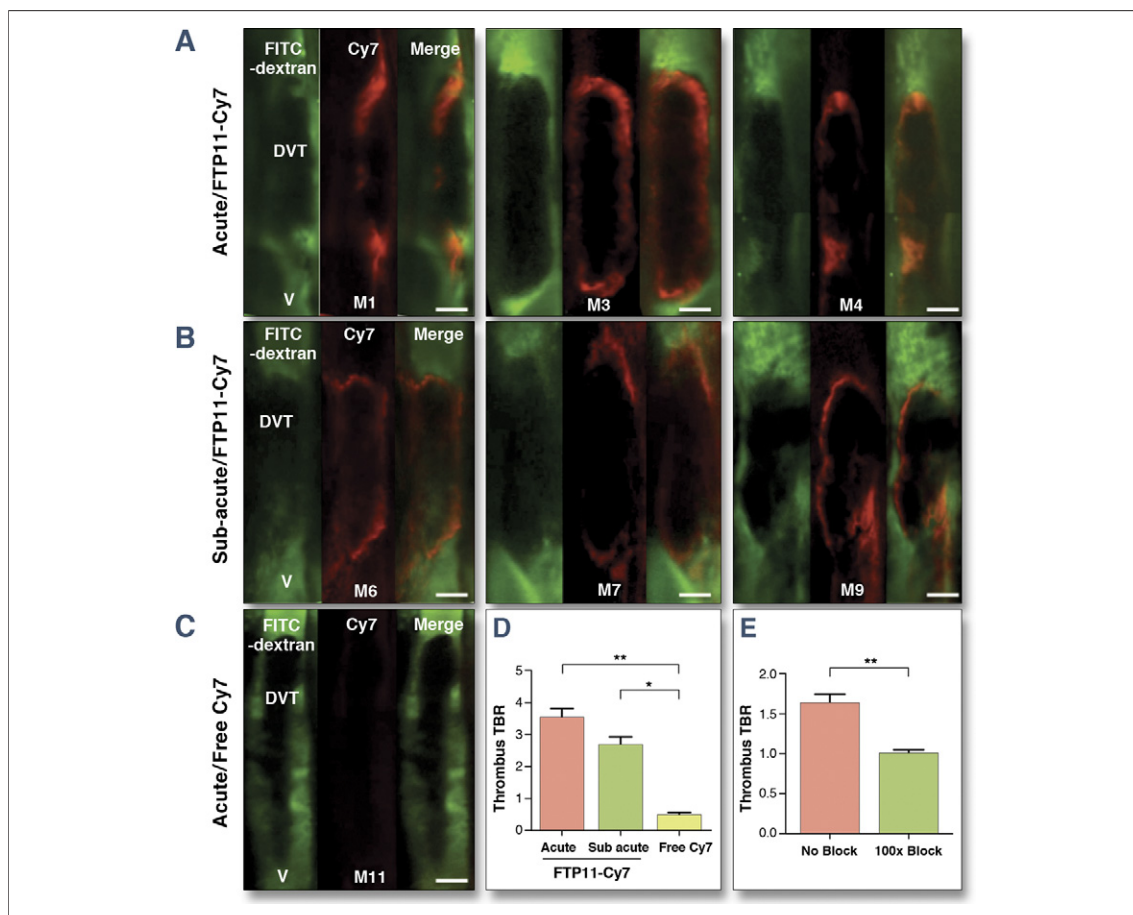
Figure 4. High-Resolution IVFM Detection of Fibrin Deposition in Femoral DVT

Femoral veins were treated with topical ferric chloride to induce deep vein thrombosis (DVT). After FTP11-Cy7 imaging agent injection, intravital fluorescence microscopy (IVFM) of **(A)** acute DVT or **(B)** subacute DVT was performed. Representative images from multiple mice in each group are shown. Both acute and subacute thrombi were enhanced by FTP11-Cy7. **(C)** In contrast, control free Cy7 did not enhance venous thrombi. **(D)** The thrombus TBR was significantly higher in the FTP11-Cy7 group compared with the control free Cy7 group. **(E)** FTP11-Cy7 based NIRF signal deposition in acute thrombi was blocked by pre-injection of a 100-fold excess of unlabeled FTP11. *p < 0.05, **p < 0.001. Scale bars, 100 μm. FITC = fluorescein isothiocyanate; V = vein; other abbreviations as in Figure 2.

IVFM enabled high-resolution in vivo detection of fibrin in both acute and subacute murine DVT, with significantly greater thrombus-to-background ratios compared with controls. In vitro and in vivo blocking studies further demonstrated that FTP11-Cy7 was thrombus specific. Capitalizing on the multispectral capabilities of IVFM, fibrin-rich thrombi were actively detected by FTP11-Cy7 enhancement and passively corroborated by FITC-dextran angiography. In vivo, the NIRF fibrin-targeted agent bound to the luminal surface of thrombus and did not penetrate the deep interior of the clot, despite its relatively small molecular weight, consistent with greater thrombus organization in the deeper (older) regions of thrombi.

Given these data, the validated NIRF fibrin-imaging agent FTP11-Cy7 may prove to be a valuable asset in investigations that aim to track and quantify fibrinogenesis and fibrinolysis in vivo, especially in murine model systems. Compared with an antibody-based imaging agent that required pre-injection (21), the NIRF fibrin-targeted agent is readily synthesizable, provides good thrombus TBRs in rapid fashion due its favorable pharmacokinetics, and demonstrates utility for acute and subacute DVT. In contrast to other fibrin-imaging agents for in vivo NIRF molecular imaging of thrombosis (16), the current peptide-based fibrin agent provides improved thrombus TBRs in subacute thrombi in addition to acute thrombi, consistent with its high binding affinity to fibrin (8).

The NIRF fibrin-targeted agent also enabled noninvasive FMT imaging of fibrin in murine jugular DVT. FMT is a 3-dimensional, quantitative
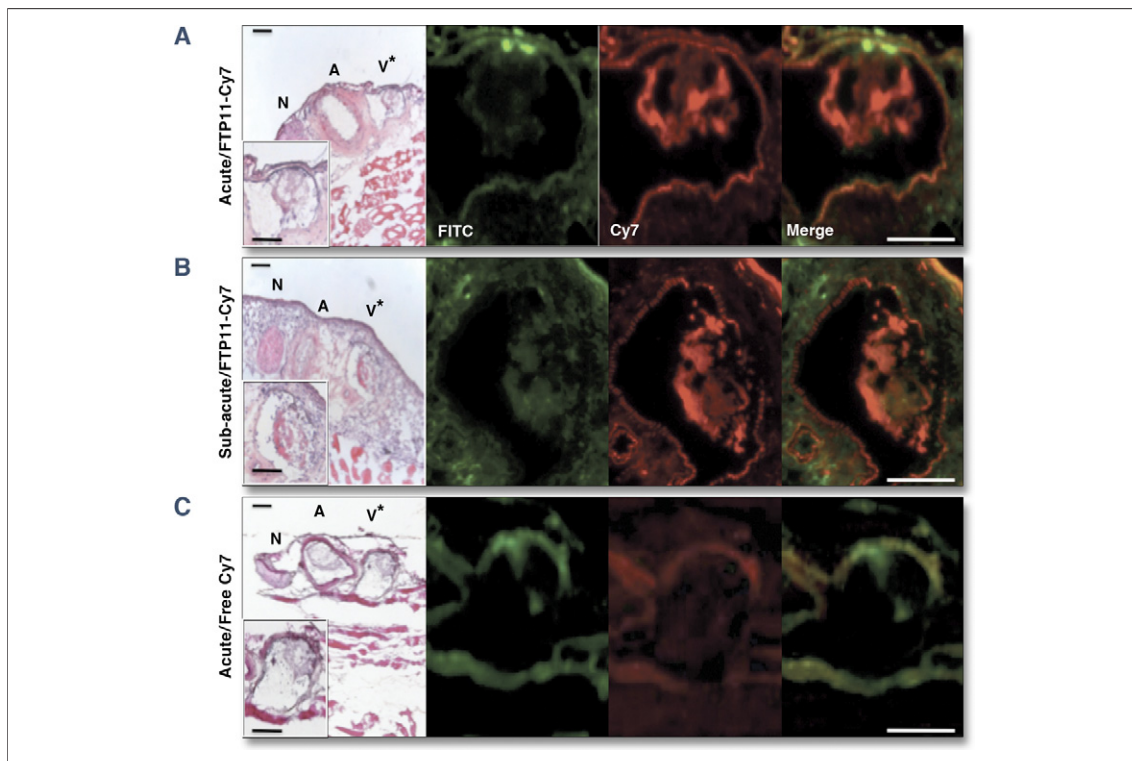
Figure 5. Thrombus-Specific Binding of FTP11-Cy7 in Murine Venous Thrombi

Fluorescence microscopy and hematoxylin and eosin (H&E) photomicrographs. Fluorescein isothiocyanate (FITC) **(green)**, Cy7 **(red)**, merged image (FITC + Cy7), and H&E are shown in each **panel**. FTP11-Cy7 accumulated into both **(A)** acute and **(B)** subacute thrombus. **(C)** In contrast, free Cy7 did not bind thrombus. **Lower left panel** shows enlarged thrombosed vein. Scale bars, 100 μm.

tomographic imaging technique that allows recon-struction of NIR deep within the body by using an array of photon detectors and inversion algorithms (12). The addition of CT, similar to integrated single-photon emission CT or positron emission tomography–CT systems, allows further co-
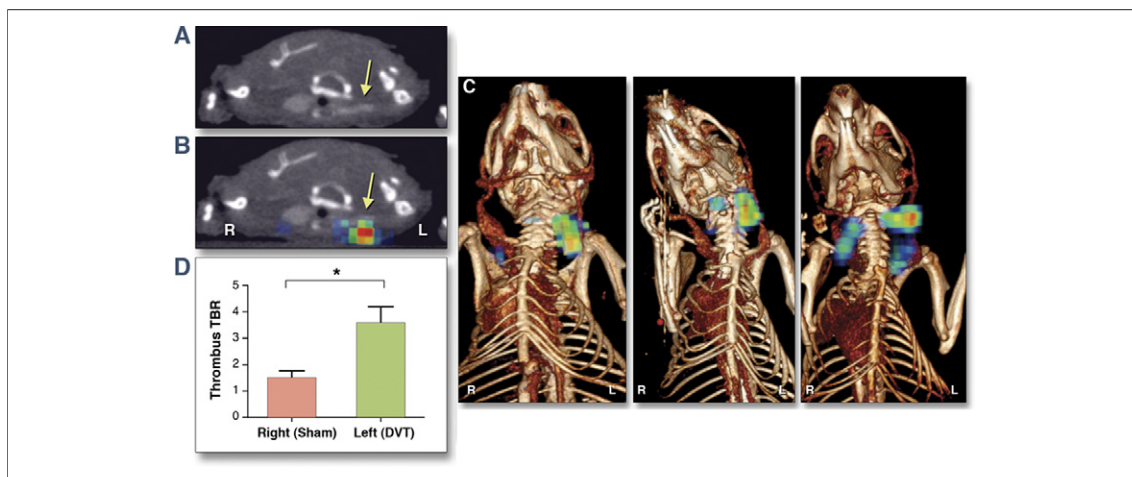
Figure 6. Noninvasive Molecular Imaging of Fibrin in Jugular DVT by Integrated FMT-CT

In C57BL/6 mice, the left jugular vein was treated with ferric chloride to induce DVT and then fluorescence molecular tomography–computed tomography (FMT-CT) was performed at day 3. **(A, B)** CT- and FMT-CT co-registered images of 2-dimensional fusion and **(C)** 3-dimensional fusion are shown. **Arrows** indicate a thrombosed left jugular vein. **(D)** The TBR of thrombosed jugular veins was significantly higher than sham-operated jugular veins (*p < 0.05) of 9 mice. Other abbreviations as in Figure 4.

Figure 7. Ex Vivo Targeting of FTP11-Cy7 to Thrombosed Jugular Veins

(A) Fluorescence reflectance image of Cy7 channel and **(B)** ex vivo image of color photograph. High NIRF signal in jugular vein is matched to the thrombosed lesion. **(C)** The thrombus TBR of the left thrombosed jugular vein was 50% greater than the sham-operated right jugular vein (*$p < 0.05$) in 9 mice. **Arrows** indicate a thrombosed left jugular vein. Abbreviations as in Figure 4.

registration using high-resolution anatomic information. In vivo investigations demonstrated the ability to image fibrin in subacute jugular DVT, with NIRF signal co-localizing with occluded veins on CT venography (Fig. 6). Sham surgery–treated veins demonstrated significantly less NIR fluorescence. Modest fibrin signal in the healing incision was also noted and expected as fibrin formation occurs during normal wound healing (22). The ability to track and quantify fibrin deposition noninvasively in DVT offers the potential to serially investigate therapies that modulate fibrin within thrombi, and could provide insights into DVT resolution and the risk of developing post-thrombotic syndrome (23,24). From a translational perspective, larger FMT or optoacoustic systems scalable to size of the human leg are feasible (25) and thus may eventually enable clinical NIRF imaging of fibrin within DVT. In addition, such systems could be harnessed to image fibrin content in carotid plaques to inform stroke risk at baseline and during carotid arterial intervention (e.g., stenting, endarterectomy).

A more immediate clinically relevant application of the fibrin-targeted NIRF agent is intravascular NIRF imaging of fibrin deposition on implanted coronary stents. Intravascular NIRF imaging is a new high-resolution strategy to image molecular and cellular aspects of vascular disease (13,14,26). Via optimized optical fiber catheters, intravascular NIRF imaging can provide high-resolution, sensitive readouts of molecular targets in coronary-sized vessels through blood, without the need for flushing, due to relatively low blood attenuation of NIR light. In the future, the ability to image fibrin on healing coronary stents may offer new insights into the pathogenesis of stent thrombosis, particularly late

stent thrombosis in current and next-generation drug-eluting stents, especially when coupled with high-resolution structural imaging via intravascular ultrasound (14) or via single catheters integrating NIRF with optical frequency domain imaging (27), a leading modality for imaging coronary stent architecture.

Study limitations. The free cyanine dye (free Cy7) and unlabeled competing FTP11 peptide were used as controls in all experiments. Although a peptide-based control agent (e.g., scrambled peptide-Cy7) could have additionally been used, previous publications have validated the specificity of the fibrin-targeting peptide backbone (FTP11) used in this study (5-8,10). Higher blocking peptide concentrations could provide greater blocking effects. In addition, dose- and time-optimization experiments of FTP11-Cy7 could yield higher thrombus TBRs than currently achieved.

CONCLUSIONS

A new synthesized NIRF fibrin-targeted peptide was found to avidly and specifically bind murine and human thrombi, and enable sensitive, fast multimodal intravital and noninvasive optical imaging detection of acute and subacute murine DVT in vivo.

Reprint requests and correspondence: Dr. Farouc A. Jaffer, Simches Research Building, Room 3206, Cardiovascular Research Center, Massachusetts General Hospital, 185 Cambridge Street, Boston, Massachusetts 02114. *E-mail: fjaffer@mgh.harvard.edu.*

REFERENCES

1. Roger VL, Go AS, Lloyd-Jones DM, et al. Heart disease and stroke statistics—2011 update: a report from the American Heart Association. Circulation 2011;123:e18–209.

2. Ciesienski KL, Caravan P. Molecular MRI of thrombosis. Curr Cardiovasc Imaging Rep 2010;4:77–84.

3. Taillefer R. Radiolabeled peptides in the detection of deep venous thrombosis. Semin Nucl Med 2001;31:102–23.

4. Morris TA. SPECT imaging of pulmonary emboli with radiolabeled thrombus-specific imaging agents. Semin Nucl Med 2010;40:474–9.

5. Sirol M, Fuster V, Badimon JJ, et al. Chronic thrombus detection with in vivo magnetic resonance imaging and a fibrin-targeted contrast agent. Circulation 2005;112:1594–600.

6. Uppal R, Ay I, Dai G, Kim YR, Sorensen AG, Caravan P. Molecular MRI of intracranial thrombus in a rat ischemic stroke model. Stroke 2010;41:1271–7.

7. Botnar RM, Buecker A, Wiethoff AJ, et al. In vivo magnetic resonance imaging of coronary thrombosis using a fibrin-binding molecular magnetic resonance contrast agent. Circulation 2004;110:1463–6.

8. Overoye-Chan K, Koerner S, Looby RJ, et al. EP-2104R: a fibrin-specific gadolinium-based MRI contrast agent for detection of thrombus. J Am Chem Soc 2008;130:6025–39.

9. Spuentrup E, Botnar RM, Wiethoff AJ, et al. MR imaging of thrombi using EP-2104R, a fibrin-specific contrast agent: initial results in patients. Eur Radiol 2008;18:1995–2005.

10. Vymazal J, Spuentrup E, Cardenas-Molina G, et al. Thrombus imaging with fibrin-specific gadolinium-based MR contrast agent EP-2104R: results of a phase II clinical study of feasibility. Invest Radiol 2009;44:697–704.

11. Chang K, Francis SA, Aikawa E, et al. Pioglitazone suppresses inflammation in vivo in murine carotid atherosclerosis: novel detection by dual-target fluorescence molecular imaging. Arterioscler Thromb Vasc Biol 2010;30:1933–9.

12. Ntziachristos V, Tung CH, Bremer C, Weissleder R. Fluorescence molecular tomography resolves protease activity in vivo. Nat Med 2002;8:757–60.

13. Jaffer FA, Vinegoni C, John MC, et al. Real-time catheter molecular sensing of inflammation in proteolytically active atherosclerosis. Circulation 2008;118:1802–9.

14. Jaffer FA, Calfon MA, Rosenthal A, et al. Two-dimensional intravascular near-infrared fluorescence molecular imaging of inflammation in atherosclerosis and stent-induced vascular injury. J Am Coll Cardiol 2011;57:2516–26.

15. Jaffer FA, Libby P, Weissleder R. Optical and multimodality molecular imaging: insights into atherosclerosis. Arterioscler Thromb Vasc Biol 2009;29:1017–24.

16. McCarthy JR, Patel P, Botnaru I, Haghayeghi P, Weissleder R, Jaffer FA. Multimodal nanoagents for the detection of intravascular thrombi. Bioconjug Chem 2009;20:1251–5.

17. Jaffer FA, Tung CH, Wykrzykowska JJ, et al. Molecular imaging of factor XIIIa activity in thrombosis using a novel, near-infrared fluorescent contrast agent that covalently links to thrombi. Circulation 2004;110:170–6.

18. Veilleux IS, Biss JA, Cote D, Lin CP. In vivo cell tracking with video rate multimodality laser scanning microscopy. IEEE J Sel Top Quantum Electron 2008;14:10–8.

19. Nahrendorf M, Waterman P, Thurber G, et al. Hybrid in vivo FMT-CT imaging of protease activity in atherosclerosis with customized nanosensors. Arterioscler Thromb Vasc Biol 2009;29:1444–51.

20. Miserus RJ, Herias MV, Prinzen L, et al. Molecular MRI of early thrombus formation using a bimodal alpha2-antiplasmin-based contrast agent. J Am Coll Cardiol Img 2009;2:987–96.

21. Falati S, Gross P, Merrill-Skoloff G, Furie BC, Furie B. Real-time in vivo imaging of platelets, tissue factor and fibrin during arterial thrombus formation in the mouse. Nat Med 2002;8:1175–81.

22. Singer AJ, Clark RA. Cutaneous wound healing. N Engl J Med 1999;341:738–46.

23. Henke PK, Wakefield T. Thrombus resolution and vein wall injury: dependence on chemokines and leukocytes. Thromb Res 2009;123 Suppl 4:S72–8.

24. Wakefield TW, Myers DD, Henke PK. Mechanisms of venous thrombosis and resolution. Arterioscler Thromb Vasc Biol 2008;28:387–91.

25. Ntziachristos V, Razansky D. Molecular imaging by means of multispectral optoacoustic tomography (MSOT). Chem Rev 2010;110:2783–94.

26. Vinegoni C, Botnaru I, Aikawa E, et al. Indocyanine green enables near-infrared fluorescence imaging of lipid-rich, inflamed atherosclerotic plaques. Sci Transl Med 2011;3:84ra45.

27. Yoo H, Kim JW, Shishkov M, et al. Intra-arterial catheter for simultaneous microstructural and molecular imaging in vivo. Nat Med 2011;17:1680–4.

Key Words: DVT ■ fibrin ■ fluorescence ■ molecular imaging ■ optical imaging.

▶ **APPENDIX**

For the full synthesis details, please see the online version of this article.